

Topological friction in a Kitaev chain heat engine

Elif Yunt,^{1, 2, *} Mojde Fadaie,^{3, 2, †} Özgür E. Müstecaplıoğlu,^{2, ‡} and Cristiane Morais Smith^{4, §}

¹*Department of Physics, University of Malta, Msida MSD 2080, Malta*

²*Department of Physics, Koç University, 34450 Sarıyer, Istanbul Turkey*

³*Department of Physics, Université de Montréal,*

1375 Avenue Thérèse-Lavoie-Roux, Montreal, Canada

⁴*Institute for Theoretical Physics, Utrecht University,*

Princetonplein 5, 3584 CC Utrecht, The Netherlands

We investigate a heat engine with a finite-length Kitaev chain in an ideal Otto cycle. It is found that the critical point of the topological phase transition coincides with the maxima of the efficiency and work output of the total Otto engine. Finite size effects are taken into account using the method of Hill's nanothermodynamics, as well as using the method of temperature-dependent energy levels. We identify the bulk and boundary thermal cycles of the Kitaev chain engine and find that they are non-ideal Otto cycles. The physics of deviation from ideal Otto cycle is identified as a finite size effect, which we dub as "topological friction", leading to heat transfer from the bulk to the boundary during adiabatic transformation of the whole system. Besides, we have determined the regimes allowing for independently running an ideal Otto refrigerator at the boundary and ideal Otto engines in the bulk and in the whole system. Furthermore, we show that the first-order phase transition in the boundary and the second-order phase transition in the bulk can be identified through their respective contributions to the engine work output.

I. INTRODUCTION

Thermodynamic methods are strictly applicable only to describe energy processes of macroscopically large objects. Progress in engineering ever smaller energy devices makes the question of how to extend the scope of thermodynamics to finite-size structures increasingly significant. For macromolecules, such as polymers, a formulation of thermodynamics has been proposed in the early 1960s by T. L. Hill [1, 2], and was later named as nanothermodynamics [3–5]. Its general principles have been also applied to other finite-size systems. In particular, topological phase transitions have been studied using the nanothermodynamic approach [6, 7] and a relation to the Uhlmann phase [8, 9] has been pointed out. Non-trivial heat transport effects, such as chiral heat currents in topological phases, has been discussed in [10]. In addition, for a topological Kondo insulator, nanothermodynamics predicts a negligible boundary effect on the anomalous heat capacity [11]. Recent studies suggest that gap-closing topological phase transitions can be probed using the work output of quantum heat engines [12]. Here, we ask whether similar conclusions can be reached in the presence of finite-size effects and examine a nanothermodynamic heat engine of a finite-length Kitaev chain [13].

The Kitaev chain exhibits a topological phase transition (TPT) from a trivial to a topological phase, in which it hosts topological zero-energy Majorana modes localized at the edges. The non-Abelian braiding statistics of these Majorana zero modes are appealing for topological

quantum computation [14]. Due to the challenges concerning their direct observation, indirect probing schemes have been discussed [15]. An interesting proposal is to utilize stroboscopic heat current in a time periodic modulated spin chain to detect signatures of Floquet-Majorana modes [16]. Our scheme addresses a static Kitaev chain and allows for a rigorous treatment of heat transfer into the system by taking into account finite-size effects using nanothermodynamic methods and by considering the interface effects of the thermal environment on the energy spectrum of the finite chain.

At the heart of Hill's nanothermodynamics lies the consideration of a macroscopic ensemble of equivalent, identical, and non-interacting small systems. The energy cost to add or remove one of these small systems, keeping their volume, mean number, and entropy constant, is associated with the so-called subdivision potential [1, 2]. An alternative formulation of the thermodynamics of a system smaller than its surroundings is based upon the idea of perturbation of the system spectrum by the thermal environment [17, 18]. Canonical thermalization of the small system at the environment temperature can be properly explained by applying a method of temperature dependent energy levels (TDELs) [19–21]. Hill's nanothermodynamics and the method of TDELs can be connected to each other by recognizing the subdivision potential to be a thermal perturbation produced by the environment [19]. We use the TDEL in conjunction with Hill's nanothermodynamics and show that the TDEL method predicts a different amount of heat exchange between the heat bath and the system than Hill's nanothermodynamics, as it takes into account the contribution of the bath-system interface as another energy dissipation channel [22, 23], consistent with the extended second law of thermodynamics [24]. Similar to the analysis of heat-transfer efficiency in thermoelectric devices with TDELs [23], here we exam-

* elif.yunt@um.edu.mt

† Seyedeh.mozhdeh.fadaie@umontreal.ca

‡ omustecap@ku.edu.tr

§ c.demoraissmith@uu.nl

ine the effects of system-bath interface in the operation of a topological nanothermodynamic heat engine.

Using Hill's nanothermodynamic methods, we distinguish the bulk and boundary contributions in the Kitaev chain Otto engine. An Otto cycle consists of isentropic (adiabatic) and isochoric (more generally isoparametric) stages. We find that when the whole system runs in an ideal Otto cycle, bulk and boundary undergo their own non-ideal Otto cycles. The conservation of the entropy of the total system in the adiabatic stages cannot warrant constant entropy for the bulk and the boundary so that the engine or the refrigerator cycles for the bulk and the boundary may differ from an Otto cycle. We found that there is a heat transfer from the bulk to the boundary during the adiabatic stages of the Otto cycle of the whole system that cause deviations from the ideal Otto cycle for the bulk and boundary. We dub the effect as a “topological friction”, being a finite size (or spatial) analog of the finite time “internal friction” [25]. In addition, we point out that for a certain parameter range in the topological phase, either only the bulk or only the boundary can be transformed in an ideal Otto cycle.

It is known that the Kitaev chain undergoes a second-order phase transition at the bulk and a first-order phase transition at the boundary [6]. We are able to identify the order of the topological phase transition in the work output of the topological heat engine by drawing an analogy of the boundary and bulk contributions with the quantum phase transitions of the Landau-Zener model in the cases of level crossing and avoided crossing, respectively.

When we adopt the TDEls approach, the heat exchange between the bath and the chain is modified, consistent with the generalized second law. The input heat is reduced and output heat is enhanced in the engine operation, resulting in a decrease in the overall work output when the energy loss in the system-bath interface is taken into account.

This paper is organized as follows. We briefly review the Hill's nanothermodynamics and the framework of TDEls that we use in two subsections in Sec. II. Our model system, the finite-length Kitaev Chain is presented in Sec. III. The results and discussions are given in Sec. IV in four subsections. We conclude in Sec. V. In the appendix A, we elaborate on the Landau-Zener and spin-1/2 quantum heat engines and establish the analogy to bulk and boundary contributions in the Kitaev heat engine.

II. METHODS

We summarize here the key points of two major historical approaches to extend the thermodynamic description to finite size systems: (i) Hill's nanothermodynamics [1] and (ii)TDEls [19, 22, 23]. We shall restrict ourselves to these two general methods to develop our results. There are also other approaches to describe the thermodynamics of small systems, but they are beyond the scope of the present paper [26–28].

A. Hill's Nanothermodynamics

In finite systems, the extensivity of the free energy is broken due to boundary effects. Hill's idea is to consider an ensemble of equivalent, identical and non-interacting small systems, so that ordinary thermodynamics can be used by introducing a so-called subdivision potential, ϵ to represent the energy cost of adding another small-system replica to the ensemble.

Let us assume that the ensemble is a grand-canonical one, in an environment characterized by temperature T and chemical potential μ . The Gibbs differential relation of the ordinary thermodynamics can now be employed to write

$$dE_t = TdS_t - pMdV + \mu dN_t + \epsilon dM, \quad (1)$$

where M is the number of replicas of the small system, and each of them has volume V and pressure p . The total internal energy, entropy, and the number of the particles in the ensemble are denoted by E_t , S_t , and N_t , respectively. The ϵ in the last term could be interpreted as a “system” chemical potential or as the work done by expanding the ensemble by adding another replica to it. For the latter, the “integral pressure”, \hat{p} is defined by Hill [2], by taking ϵ as the grand potential of a single system, with $\epsilon = -\hat{p}V$.

Integrating Eq. (1) by the Euler theorem, for fixed T, p, μ, ϵ , and then dividing the result by M , we find

$$E = TS - pV + \mu N + X. \quad (2)$$

Here, E and N are the mean energy and mean number of particles for a single small system in the ensemble, while S is the entropy, which is the same for each small system [1, 2]. Due to the last term $X := (p - \hat{p})V$, which is called subdivision potential, E is not a linear homogeneous function of S, V, N . In general, \hat{p} is size dependent, but the leading order term is independent of V . The extensivity is broken, while the ordinary thermodynamics can be recovered in the limit $X \rightarrow 0$. The corresponding differential Gibbs relation is then found to be

$$dE = TdS - pdV + \mu dN, \quad (3)$$

with the generalized Gibbs-Duhem equation

$$dX = -SdT + Vdp - Nd\mu, \quad (4)$$

while the differential relation for ϵ is the same as the ordinary thermodynamic one,

$$d\epsilon = -SdT - pdV - Nd\mu. \quad (5)$$

Connection to statistical mechanics can be made by

$$\epsilon = -k_B T \ln \Xi, \quad (6)$$

where

$$\Xi(\mu, T, V) = \text{Tr} \exp[-\beta(H - \mu N)], \quad (7)$$

is the grand canonical partition function for a single small system described by the Hamiltonian H in the ensemble with $\beta = 1/k_B T$.

Equations (2)-(4) constitute the essential relations of Hill's nanothermodynamics. We remark two subtle points: first, it is assumed that the small systems can be thermalized to the bath temperature T and Hill's thermodynamics does not give any mechanism for this thermal equilibration; and second, the subdivision potential is a phenomenological term presented without any microscopic origin. These two issues are going to be addressed within the framework of the TDELS method.

B. Temperature-dependent energy levels

The method of TDELS has been proposed as a fast and convenient way to perform statistical mechanical calculations for an assembly of systems [17, 18]. It has been applied to semiconductors [29–32], superfluids [33], optomechanical oscillators [34, 35], heat losses in thermoelectric systems [22, 23], and thermalization of finite-size systems [19–21]. TDELS can be associated with a temperature-dependent effective Hamiltonian, or a so called "Hamiltonian of mean force" arising as the result of a prior averaging over certain possible microstates of the assembly in thermal equilibrium [36, 37]. For example, electronic energy levels in semiconductors change with the temperature due to interaction of the electrons with the lattice, which is subject to thermal expansion [30].

In the presence of TDELS, the energy transferred from the heat bath to the system cannot be completely identified as heat. As the system temperature changes to match with that of the heat bath, the energy gaps between the energy levels may change, in addition to their populations. Writing the mean energy as $E = \langle H(T) \rangle = \text{Tr}(\rho H(T))$ and keeping all the other parameters constant, the infinitesimal mean energy change for a small system in contact with a heat bath then reads [19–23],

$$dE = TdS_T + \left\langle \frac{\partial H}{\partial T} \right\rangle dT. \quad (8)$$

Here, the first term is the heat associated with the population changes of the TDELS with the corresponding entropy S_T . When the energy gaps change with T , the second term cannot be interpreted as heat; it represents the work applied to change the energy gaps. Such a mechanism has been discussed in detail to explain thermalization of small systems [19–21] and an effective heat describing the actual heat transfer into the small system from the thermal surroundings is defined by [19, 21–23]

$$\delta Q_{\text{eff}} = \delta Q - \left\langle \frac{\partial H}{\partial T} \right\rangle dT. \quad (9)$$

This equation originates from the first law modified for a small system; rewriting it as $dS_T = dQ/T - \langle \partial H / \partial T \rangle dT/T$, one recovers the modified second law of

information transfer channels [24]. The entropy transferred from a heat source into the system through the boundary is balanced by the entropy lost at the boundary. The boundary acts as an energy channel interfacing the heat source and the system.

Hill's nanothermodynamics and the method of TDELS can be connected to each other by recognizing that the subdivision potential can be determined by [19]

$$X = T \left\langle \frac{\partial H}{\partial T} \right\rangle. \quad (10)$$

We can use the calculations of Hill's nanothermodynamics to evaluate the heat transfer as described by the TDEL method according to

$$Q_{\text{eff}} = \int TdS - \int \frac{X}{T} dT. \quad (11)$$

We emphasize that the first term is written in terms of the S of Hill's nanothermodynamics, according to which we have $dE = dQ = TdS$. The TDELS method yields a correction term associated with the work done on the energy gaps, such that some heat is dissipated at the system-bath interface and only an effective heat is received by the system.

Next, we apply this generic formalism to a specific model.

III. MODEL: KITAEV CHAIN IN OTTO CYCLE

The Kitaev chain is a one-dimensional topological superconductor model [13], which consists of spinless fermions, described by the Hamiltonian

$$H = -\mu \sum_{i=1}^n a_i^\dagger a_i - \sum_{i=1}^{n-1} (ta_i^\dagger a_{i+1} - \Delta a_{i+1} a_i + h.c.) \quad (12)$$

Here, $i = 1 \dots n$ labels the n sites on the one-dimensional finite-length Kitaev chain, μ is the chemical potential, t is the hopping parameter, and Δ is the superconducting pairing parameter. The fermionic annihilation (creation) operators, $a_i (a_i^\dagger)$ satisfy the anti-commutation relations $\{a_i, a_j^\dagger\} = \delta_{ij}$. The Kitaev chain undergoes a topological phase transition at $|\mu| = 2t$, which separates a topological phase for $|\mu| < 2t$ from a trivial phase for $|\mu| > 2t$. In the topological phase, the Kitaev chain hosts a pair of Majorana zero modes at its edges.

Following the Hill's nanothermodynamics, an ensemble of identical, equivalent, and non-interacting copies of a finite-length Kitaev chain will be considered. For the TDEL approach, we consider a macroscopic Kitaev chain decomposed into two parts: One part is taken as the finite-length system, and the other is an interface lead, which is long enough to be assumed in thermal equilibrium with a heat bath [17]. TDELS arise as a result of averaging over the interface microstates, and describe the heat exchange

during the thermalization of the finite-length chain with the heat bath in a thermodynamically consistent way.

Bulk and boundary thermodynamical properties of the finite-length Kitaev chain can be investigated using the Hill's nanothermodynamic framework. For that aim, we introduce the following ansatz for the grand potential [6]

$$\Phi(\mu, T, L) = \Phi_c(\mu, T)L + \Phi_0(\mu, T). \quad (13)$$

Here, $\Phi_c L = -pL$ is the bulk grand potential, which is extensive, while $\Phi_0 = X$ is the subdivision potential, which emerges due to the finite length of the chain. The corresponding entropies obey a similar relation,

$$S = S_c L + S_0. \quad (14)$$

The first term, the bulk entropy, coincides with the entropy of the total system in the thermodynamic limit, where S_0 disappears at $L \rightarrow \infty$. This first term can be larger than the entropy of the total finite system because S_0 can be negative. A negative S_0 is allowed in the Hill's thermodynamics, which is a non-extensive thermodynamic theory. Similar conclusions apply to other thermodynamic quantities, which are extensive in the thermodynamic limit but non-extensive in the finite-size nanothermodynamic regime.

We first find the eigenvalues of the Hamiltonian in Eq. (12), then evaluate the total entropy S of the chain. S_c and S_0 are determined by using a linear fit to S for an n -site chain (we take the unit length of the chain as 1 so that $L = n$) in the interval $200 < n < 225$. The length is chosen to be sufficiently large to make the linear fit a valid approximation [6]. Repeating the procedure for different temperatures, the $T - S$ relation is found. We will consider the thermodynamic cycle of an ideal Otto engine. The Otto cycle consists of two isentropic (adiabatic) and two isochoric (isoparametric) stages. We take the chemical potential μ as the control parameter for the Otto cycle. The $T - S$ curves at different μ will be used to determine the explicit cycle diagram and the associated work output. In the following subsections, the corresponding work and efficiency of the Kitaev chain Otto cycle will be investigated by distinguishing the bulk and boundary contributions and by considering the effect of bath-system interface as an energy channel, which modifies the heat exchange between the heat baths and the Kitaev chain.

IV. RESULTS AND DISCUSSION

In our calculations, we consider a Kitaev chain of length $n = 225$ with a superconducting pairing parameter $\Delta = 0.25$ and a hopping parameter $t = 0.25$. μ is used as the control parameter, for which a TPT takes place at $\mu = 0.5$. The energy parameters are scaled by $k_B/\hbar v = 1$, where v is the velocity of the excitations [7].

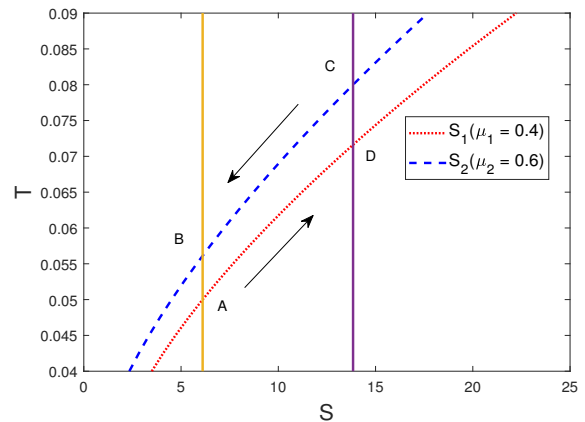


Figure 1. (Color Online) Temperature-Entropy ($T - S$) curves of a finite-length Kitaev chain according to Hill's nanothermodynamics. The chain has $n = 225$ sites and is characterized by a superconducting pairing parameter $\Delta = 0.25$ and hopping parameter $t = 0.25$. The red dotted curve is for the chemical potential $\mu_1 = 0.4$, while the blue dashed one is for $\mu_2 = 0.6$. An Otto cycle can be defined using the segments between the points A, B, C , and D determined by the intersection of the curves and the solid yellow and solid purple constant entropy lines. The cycle operates between a cold bath at temperature $T_A = 0.05$ and a hot bath at temperature $T_C = 0.08$ in the anti-clockwise direction. The arrows indicate the direction of the heat engine cycle producing positive work.

A. Work and efficiency of finite-length Kitaev chain Otto engine

Let us first consider the finite-length Kitaev chain as a whole. The $T - S$ curves of the chain at $\mu_1 = 0.4$ (red dotted) and $\mu_2 = 0.6$ (blue dashed) are plotted in Fig. 1. The vertical lines are the constant entropies $S_2(T_B) = S_1(T_A)$ and $S_2(T_C) = S_1(T_D)$, where T_x denote the temperature of the chain at the point $x = A, B, C, D$. The lines are fixed by the cold and hot bath temperatures, $T_A = 0.05$ and $T_C = 0.08$, respectively. The Otto cycle is then determined by finding the intermediate temperatures, T_B and T_D from the constant entropy conditions. By intermediate temperatures, we refer to the temperatures the total system attains between the hot and cold baths. We work in the low-temperature regime, where the temperatures in the Otto cycle are much less than the energy gap. The heat exchanges of the chain with the heat baths at the isoparametric stages $A \rightarrow D$ and $C \rightarrow B$ are calculated by

$$Q_{AD} = \int_{T_A}^{T_D} T \frac{dS_1}{dT} dT, \quad Q_{CB} = \int_{T_C}^{T_B} T \frac{dS_2}{dT} dT, \quad (15)$$

where the entropies of the chain for $\mu = \mu_1$ and $\mu = \mu_2$ are distinguished by S_1 and S_2 , respectively. The net work performed by the cycle is then calculated by $W = Q_{AD} + Q_{CB}$.

$Q_{AD} > 0 > Q_{CB}$ and the positivity of W is required for heat engine operation, while $Q_{CB} > 0 > Q_{AD}$ and a

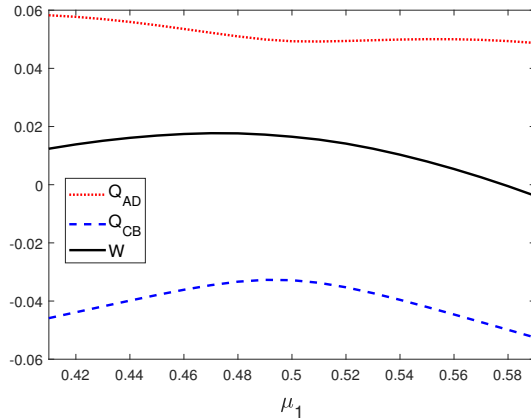


Figure 2. (Color online) The absorbed heat Q_{AD} (red dotted), the ejected heat Q_{CB} (blue dashed), and the net work output W (black solid) are given as a function of the chemical potential μ_1 of the first isochore for an ideal Otto cycle working between a cold bath at temperature $T_A = 0.05$ and a hot bath at temperature $T_C = 0.08$.

negative work output would be the case of refrigerator behavior. We use a sign convention, where heat injected to (ejected from) the system is always taken to be positive (negative).

We now fix the parameter of the second isochore $\mu_2 = 0.6$ and vary the one for the first isochore $\mu_1 \equiv \mu$ from 0.4 to 0.6. Using the construction of the Otto cycle described in Fig. 1, we evaluate the work output and the efficiency of the cycle. In Fig. 2, we plot the injected and ejected heat, together with the work output, for a range of μ_1 values. We observe that at the TPT, the work output of the cycle becomes maximum. The TPT point (or the maximum) is slightly shifted from $\mu_1 = 0.5$, possibly because the engine operates at finite temperatures, which are known to reduce the critical value of μ [7]. For this range of μ_1 , $Q_{AD} > 0$ and $Q_{CB} < 0$, so that the cycle can be properly described as a heat engine operation with $W > 0$, except for a small range $\mu_1 > 0.585$.

As shown in Fig. 3, the efficiency is maximum at the TPT. Our results show that the TPT enhances the work output of the Kitaev chain heat engine, as well as its efficiency. The existence of a TPT in a Kitaev chain at finite temperatures is restricted to a certain temperature regime [6, 8, 9], and the temperatures that we consider here remain within this limit.

B. Bulk and boundary cycles of the Kitaev chain heat engine

The Hill's nanothermodynamic framework allows us to examine the bulk and boundary contributions to the net work output of the Kitaev chain heat engine. For that

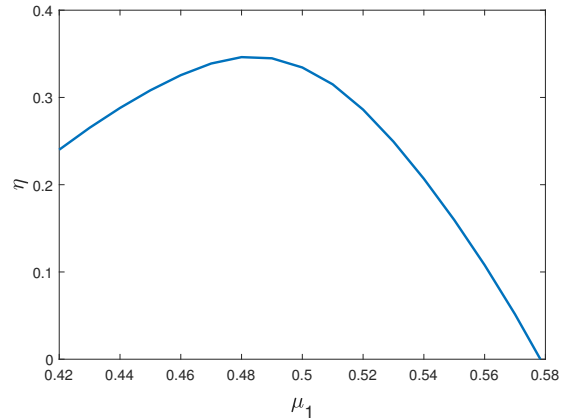


Figure 3. (Color online) The efficiency η of the finite Kitaev chain heat engine is given as a function of the chemical potential μ_1 of the first isochore for an Otto cycle working between a cold bath at temperature $T_A = 0.05$ and a hot bath at temperature $T_C = 0.08$.

aim, we use Eq. (14) to write the total heat exchange

$$Q = \int T dS = \int T dS_c L + \int T dS_0 = Q_c L + Q_0, \quad (16)$$

in terms of the bulk and boundary contributions, $Q_c L$ and Q_0 , respectively.

While the total system goes through the Otto cycle described in Fig. 1, the bulk goes through the thermal cycle plotted in Fig. 4a. The adiabatic stages are altered due to internal friction resulting from finite-size effects, and the bulk thermal cycle diverges from an ideal Otto cycle. The heat exchanges and the net bulk work output $W_c L$ are given in Fig. 4b. We find that the behavior of the heat exchanges by the bulk during the isochoric stages as a function of μ_1 are qualitatively the same as those for the entire chain heat exchanges (cf. Fig. 2).

Although there are heat exchanges during the D-C and B-A stages in the bulk, given by $Q_c^{DC} L$ and $Q_c^{BA} L$ in Fig. 4b, their effect on the bulk work output are not strong enough to change the qualitative behaviour of $W_c L$. We conclude that the bulk thermal cycle is *slightly* non-ideal Otto, and the bulk and the total system behave qualitatively similarly in their heat engine operation. The work output of the bulk engine is also maximum at the critical point of the TPT.

The bulk thermal cycle is only slightly different from the total finite Kitaev chain heat engine cycle and the dependence of the injected and ejected heat and the net work outputs on the chemical potential μ_1 do not exhibit much qualitative difference for the bulk and for the entire chain. However, the boundary behaviour is remarkably different from both.

The boundary thermal cycle is plotted Fig. 5a. This cycle produces positive work only for a small parameter range around the TPT point at $\mu_1 = 0.5$, where the boundary work, W_0 is also maximized.

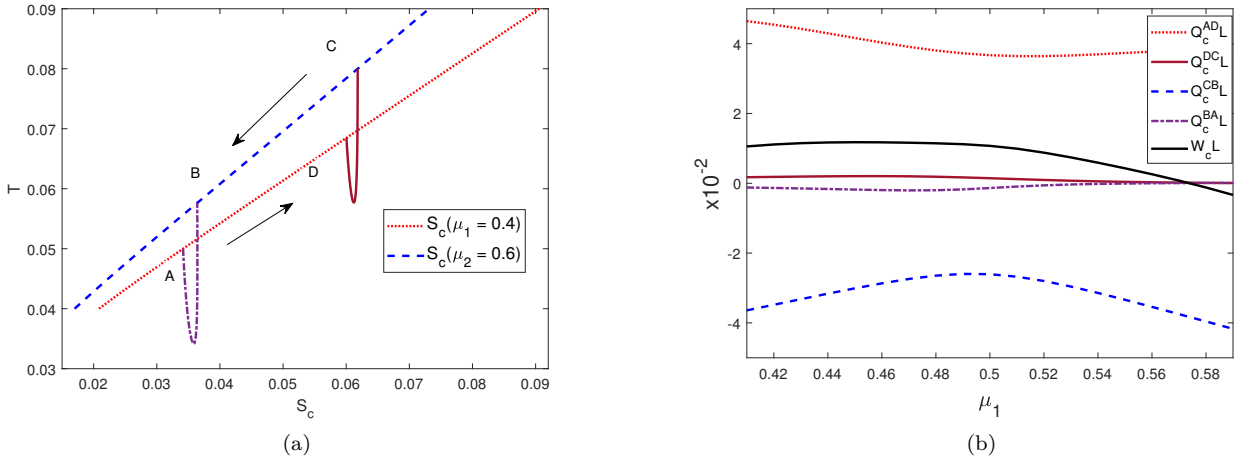


Figure 4. (Color Online) (a) The temperature-entropy density ($T - S_c$) curves for the bulk of the finite-length Kitaev chain. The red dotted curve is for the chemical potential $\mu_1 = 0.4$, while the blue dashed one is for $\mu_2 = 0.6$. There are heat exchanges on the D-C (brown solid) and B-A (purple dot-dashed) stages. (b) The heat exchanges of the bulk, $Q_c^{AD}L$ (red dotted), $Q_c^{DC}L$ (brown solid), $Q_c^{CB}L$ (blue dashed), $Q_c^{BA}L$ (purple dot-dashed), and the bulk work output W_cL (black solid) are given as a function of the chemical potential μ_1 of the first isochore of a finite-length Kitaev chain in an Otto cycle. All parameters are the same as in Fig. 1.

Inspecting both Fig. 4b and Fig. 5b, we observe that $Q_c^{BA}L = -Q_0^{BA}$ (and $Q_c^{DC}L = -Q_0^{DC}$), since there is no heat exchange in the total Kitaev chain heat engine on the adiabatic stage from point B to A (and D to C) and the LHS of Eq. 16 would be zero. The entropy flows from the bulk to the boundary, consistent with the conservation of total entropy $\Delta S = 0$. Local entropy changes in the bulk and boundary are equal and opposite to each other, $\Delta S_cL = -\Delta S_0$. While the adiabatic transformation induced by changing chemical potential is employed on the total system, heat transfer from bulk to the boundary causes deviation of ideal adiabatic transformations in either subsystem. Accordingly their cycles are non-ideal Otto cycles. This finite-size effect is a spatial analog of the finite-time imperfection of adiabatic transformations [25]. Following the term ‘internal friction’ used for imperfect finite-time adiabatic transformation in finite-time Otto cycles [25], here we dub the finite-size effect on adiabatic transformation as ‘topological friction’.

The boundary cycle shows different characteristics for the trivial ($\mu_1 > 0.5$) and topological ($\mu_1 < 0.5$) phases of the finite Kitaev chain. For the trivial phase, we can define the incoming heat as $Q_0^{\text{in}} = Q_0^{AD} + Q_0^{BA} > 0$ and the outgoing heat $Q_0^{\text{out}} = Q_0^{CB} + Q_0^{DC} < 0$ (except for some small region beyond 0.585). Then, the boundary cycle operates as a heat pump with $W_0 < 0$. In the trivial phase, the boundary and bulk thermal cycle operations are reversed. For the topological phase, the thermal cycle characteristic of the boundary cannot be identified with a heat engine or a heat pump, since the heat exchanges during both the first and second isochore, Q_0^{AD} and Q_0^{CB} respectively, are negative. It is known that the Kitaev chain exhibits a first-order phase transition at the bound-

ary and a second-order phase transition in the bulk [7]. We show in the appendix A that it is possible to probe the order of the quantum phase transition through the work output of heat engine cycles using the Landau-Zener model for a two-level system. We note here that by establishing an analogy between the boundary contribution in the Kitaev chain with the level crossing regime of the Landau-Zener model and also between the bulk contribution in the Kitaev chain with the avoided crossing regime of the Landau-Zener model, the order of the phase transition at the boundary and at the bulk of the Kitaev chain can be probed. We elaborate also on the details of this analogy in the appendix A.

Our results presented in this section show that as the total system operates in an ideal Otto cycle, the bulk of the finite Kitaev chain operates *approximately close* to an ideal Otto cycle, and the boundary is a highly peculiar non-ideal Otto cycle. In the next subsection, we address the question of whether it is possible to identify independently operating bulk, boundary, and total Otto cycles.

C. Three Otto cycles with a single finite-length Kitaev chain

In this section, we investigate whether one can find a parameter range $\mu_1 - \mu_2$ and hot and cold bath temperatures, for which bulk, boundary, and total systems could be used as working systems for Otto cycles. When one of them is chosen to work in the Otto cycle however, the other two cannot be found in the Otto cycles. It is possible to identify three independently running Otto

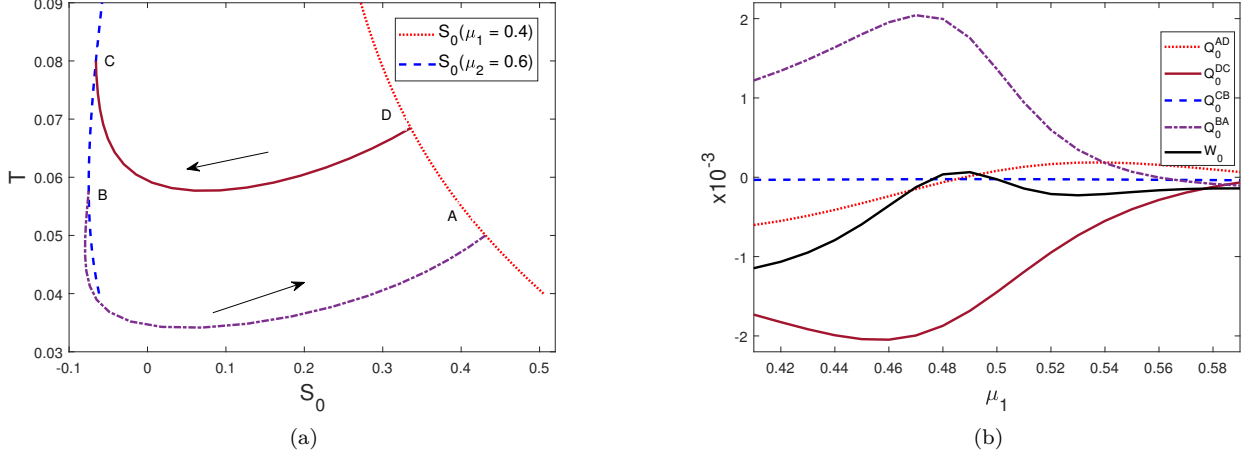


Figure 5. (Color Online) (a) The temperature-entropy ($T - S_0$) curves for the boundary of the finite-length Kitaev chain. The red dotted curve is for the chemical potential $\mu_1 = 0.4$, while the blue dashed one is for $\mu_2 = 0.6$. The process from D to C is given by the brown solid line and from B to A by the purple dot-dashed line. (b) The heat exchanges of the boundary, Q_0^{AD} (red dotted), Q_0^{DC} (brown solid), Q_0^{CB} (blue dashed), Q_0^{BA} (purple dot-dashed), and the boundary work output W_0 (black solid) are given as a function of the chemical potential μ_1 of the first isochore of a finite-length Kitaev chain in an Otto cycle. All parameters are the same as in Fig. 1.

cycles, associated with the total, bulk and boundary of the system separately. For that aim, we examine the temperature-entropy curves $T - S$, $T - S_c$, and $T - S_0$ separately. We consider the same cold and hot bath temperatures $T_A = 0.05$ and $T_C = 0.08$, respectively, for the cycles as in the previous discussions.

The Otto cycles can be determined for the bulk and for the boundary, similarly to the case of the total system. The cycles will be different due to the differences in the intermediate temperatures determined by isentropy conditions for the bulk and boundary entropies S_c and S_0 , and the entropy of the total chain S , and hence would yield different work outputs with different characteristics. In general, our numerical investigations suggest that the intermediate temperatures for the bulk and for the total system are close to each other, while the boundary can attain significantly different intermediate temperatures. We find a narrow regime in the topological phase, between $\mu_1 = 0.42$ and $\mu_2 = 0.425$ for which the boundary can produce work through an Otto cycle and act as a refrigerator.

The work outputs are shown in Figs. 6a and 6b. For the temperature and parameter range considered, the bulk behaves like an Otto heat engine, while the boundary becomes an Otto refrigerator. When we compare efficiencies of the total system and bulk heat engines, $\eta = W/Q_{AD}$ and $\eta_c = W_c/Q_c^{AD}$, respectively, as in Fig. 7, we observe that the bulk is more efficient than the total system. The efficiency of the boundary heat pump $\kappa_0 = Q_0^{CB}/|W_c|$ is given in the inset of Fig. 7.

D. Effective Work

For the TDEL approach, we consider a macroscopic Kitaev chain decomposed into two parts: One part is taken as the finite-length system, and the other is an interface lead, which is long enough to be assumed in thermal equilibrium with a heat bath [17]. TDELs arise as a result of averaging over the interface microstates, and describe the heat exchange during the thermalization of the finite-length chain with the heat bath in a thermodynamically consistent way. The TDELs method, different from Hill's approach, describes the boundary as an energy channel interfacing the bath and the system.

The connection between Hill's nanothermodynamics and TDELs is sustained by recognizing that the subdivision potential acts as a thermal perturbation by the environment. As explained in Sec. II B, the subdivision potential of Hill's nanothermodynamics can be used to calculate the heat dissipated through this boundary energy channel, upon associating $X = \Phi_0$ in Eq. (11) [19]. Thus, we use these two nanothermodynamic approaches in conjunction with each other.

The effective incoming and outgoing heats are computed, respectively, according to the following formulae:

$$Q_{AD(\text{eff})} = \int_{S_A}^{S_D} T dS - \int_{T_A}^{T_D} \frac{\Phi_0}{T} dT, \quad (17)$$

$$Q_{CB(\text{eff})} = \int_{S_C}^{S_B} T dS - \int_{T_C}^{T_B} \frac{\Phi_0}{T} dT. \quad (18)$$

The second terms in Eqs.(17-18) are the correction terms, which are computed using Φ_0 of Hill's nanothermodynam-

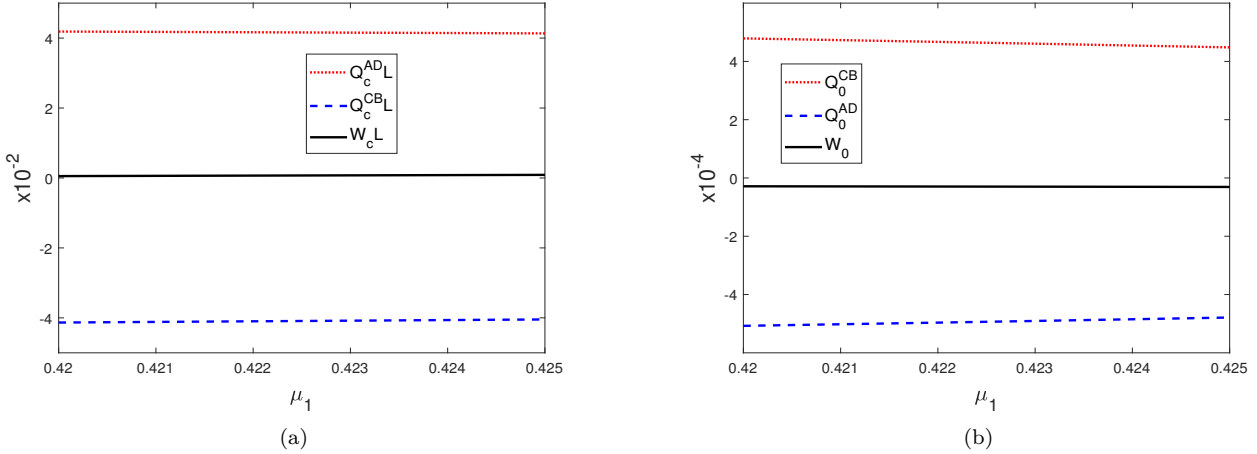


Figure 6. (Color online) The injected heat $Q_c^{AD}L$, Q_0^{CB} (red dotted) and ejected heat, Q_c^{CB} , Q_0^{AD} (blue dashed) and the work output W_c , W_0 (black solid) corresponding to (a) the bulk heat engine and (b) the boundary refrigerator, respectively, as a function of the chemical potential μ_1 of the first isochore of a finite-length Kitaev chain in independent Otto cycles, operating between a cold bath at temperature $T_A = 0.05$ and a hot bath at temperature $T_C = 0.08$ in the parameter range between $\mu_1 = 0.42$ and $\mu_2 = 0.425$. Note that the intermediate temperatures for each engine would be different due to different entropy values leading to different isoentropy conditions.

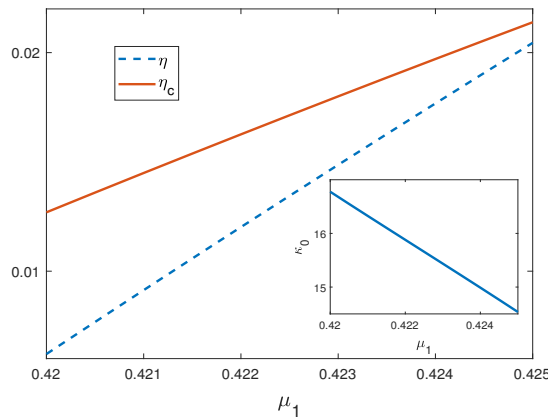


Figure 7. (Color online) The efficiencies of the total Otto heat engine η (blue dashed) and the bulk Otto heat engine η_c (red solid) are given as a function of the chemical potential μ_1 of the first isochore of a finite-length Kitaev chain in independent Otto cycles, operating between a cold bath at temperature $T_A = 0.05$ and a hot bath at temperature $T_C = 0.08$ in the parameter range between $\mu_1 = 0.42$ and $\mu_2 = 0.425$. In the inset, the coefficient of performance of the boundary Otto refrigerator κ_0 is given.

ics. The total effective work is

$$W_{\text{eff}} = Q_{\text{AD}(\text{eff})} + Q_{\text{CB}(\text{eff})}. \quad (19)$$

We calculate the injected and ejected effective heat and also the effective work for the Otto cycle depicted in Fig. 1 using Eqs. (17)-(19). The results are plotted in Fig. 8a.

There is a signature of a TPT in both $Q_{\text{AD}(\text{eff})}$, $Q_{\text{BC}(\text{eff})}$ and in the effective work W_{eff} at $\mu = 2t$. We also present

a comparison between the work calculated using Hill's nanothermodynamics and the effective work, which accounts for the TDELS in Fig. 8b. Both the work and the effective work have qualitatively the same behavior, but the effective work W_{eff} acquires lower values. The behavior of the exchanged heat values yielded by Hill's nanothermodynamics are compared with the effective heat values in Fig. 9. We observe that $Q_{\text{AD}(\text{eff})}$ is less than Q_{AD} and $Q_{\text{CB}(\text{eff})}$ is higher than Q_{CB} . This shows that the heat exchanges are modified by the interface effects taken into account through the TDELS. We note that the qualitative behaviour of heat exchanges and work outputs are the same in both approaches and that there is only a small quantitative difference.

V. CONCLUSIONS

We propose a heat engine, which uses the finite Kitaev chain as its working substance. The heat engine is based on an Otto cycle, where there are two isentropic (adiabatic) and two isochoric (isoparametric) stages. The control parameter in the engine is the chemical potential of the Kitaev chain. We work in the low temperature regime, such that the temperatures are smaller than the energy gap of the system.

We report that the TPT of the finite Kitaev chain enhances both the total work output and the efficiency. We further investigate the thermodynamic properties of the finite-length Kitaev chain within two thermodynamic frameworks for finite-size systems: Hill's nanothermodynamics and TDELS scheme.

Based on Hill's nanothermodynamics, we identify the

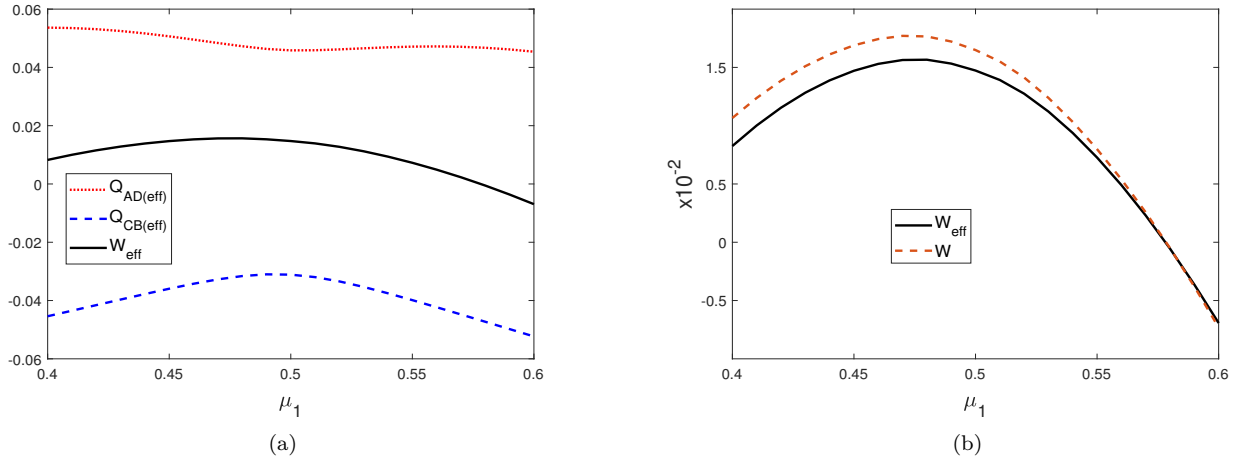


Figure 8. (Color online) (a) Effective incoming heat $Q_{AD(eff)}$ (red dotted), effective outgoing heat $Q_{CB(eff)}$ (blue dashed) and effective work W_{eff} (black solid). (b) Total net work W (red dashed) and effective work W_{eff} (black solid) are given as a function of μ_1 for an Otto cycle working between a cold bath at temperature $T_A = 0.05$ and a hot bath at temperature $T_C = 0.08$.

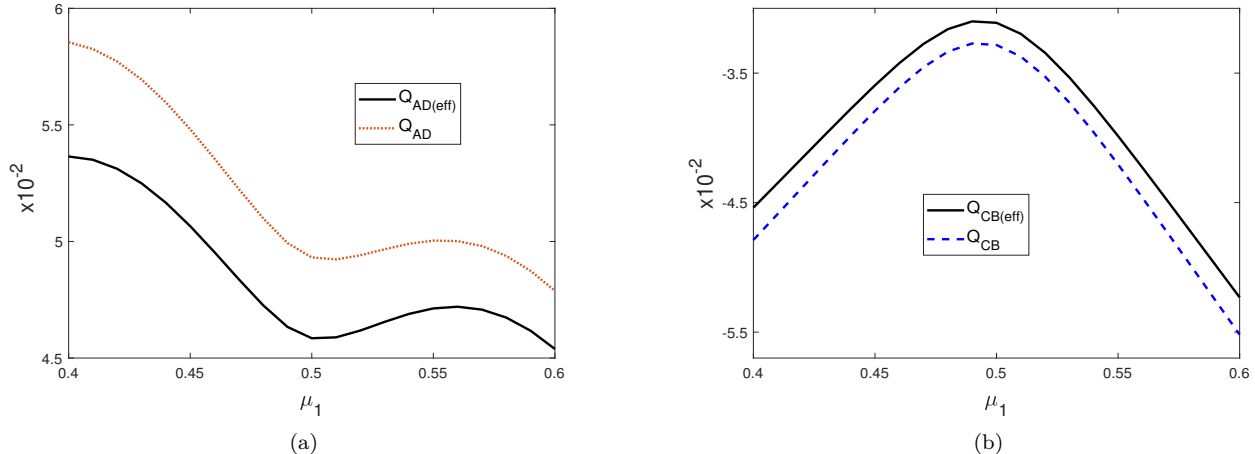


Figure 9. (Color online) (a) Absorbed heat Q_{in} (blue dashed) and effective absorbed heat $Q_{in(eff)}$ (black solid). (b) Ejected heat Q_{out} (red dotted) and effective ejected heat $Q_{out(eff)}$ (black solid) are given as a function of μ_1 for an Otto cycle working between a hot bath at temperature $T_B = 0.08$ and a cold bath at temperature $T_D = 0.05$.

separate qualitative and quantitative features arising from the bulk and boundary in the work output of the Otto cycle. We find that bulk and boundary undergo their own thermal cycles different from the ideal Otto cycle. The bulk operates in a non-ideal Otto heat engine in both phases of the Kitaev chain with a behaviour that is qualitatively similar to the one of the total system. The boundary cycle yields a positive work output only in a small parameter region around the TPT. The boundary shows two different thermal cycle characters before and after the transition point, associated with its first-order TPT behavior. The thermal cycle of the boundary contribution can be identified with neither a heat engine nor a refrigerator in the topological phase but acts as a refrigerator in the trivial phase of the finite Kitaev chain.

We conclude that the non-ideal Otto cycle behavior, which arises at the bulk and boundary is a finite-size effect, a spatial analog of the finite time internal friction (or quantum friction) [25]. Both finite-time and finite-size effects cause imperfect adiabatic transformation, leading to non-ideal Otto cycles.

We also show the existence of three Otto cycles working independently between two baths and making use of the total, bulk and boundary contribution separately. This scheme only works in the *topological* phase of the Kitaev chain. While the total system and the bulk operate as heat engines, the boundary operates as a *heat pump*. We remark that these cycles attain different intermediate temperatures and cannot be designed to operate simultaneously. Nevertheless, the Kitaev chain can be used as a

multi-functional thermal device in which engine and refrigerator operations are tunable and spatially separated to the bulk and the boundary.

Using the TDEls scheme in conjunction with the Hill nanothermodynamics approach, we have, in addition, calculated the effective heat exchange and the effective work of the finite Kitaev chain engine. We find that the effective work is qualitatively lower than what is calculated by Hill's nanothermodynamics. The incoming heat is reduced and the outgoing heat is increased due to the energy dissipation in the system-bath interface. While Hill's nanothermodynamics allows for a clear identification of the bulk and boundary contributions in the heat engine operation, TDEls provides a proper assignment of the heat exchange between the heat baths and the finite system. We show that these two approaches complement each other and can be used in conjunction for detailed modeling of thermal machines and experiments with topological finite systems.

We show that, by separating the bulk and boundary contributions to the work output of the Kitaev heat engine, we can identify the order of the phase transition taking place by inspecting these contributions. The boundary exhibits a first-order phase transition, analogous to the level crossing regime of a two-level Landau-Zener model, and the bulk exhibits a second-order phase transition like in the avoided crossing regime of the Landau-Zener model. We state a reservation in this analogy which we leave for further study, which is that the bulk and boundary of the Kitaev heat engine go through their own thermodynamic cycles, which are non-ideal Otto cycles, but still exhibit phase transition features. We note that this may be due to the universal feature of phase transitions and conclude that the phase transition features seem to be independent of the cycle being considered.

ACKNOWLEDGEMENTS

We acknowledge support by the Scientific and Technological Research Council of Turkey (TÜBİTAK), Grant No. (117F097) and by the EU-COST Action (CA16221). E.Y. would like to acknowledge A. Tuncer for helpful discussions. The authors would like to thank S.N. Kempkes and R. Arouca for a careful reading of the manuscript.

Appendix A: Landau-Zener and Spin-1/2 Model Quantum Heat Engines

We show in this appendix how quantum phase transitions of the Landau-Zener model, both in the case of level crossing and avoided crossing, are probed via a quantum Otto heat engine cycle. We draw an analogy between the bulk/ boundary contributions to the Kitaev heat engine and avoided/level crossing cases of a Landau-Zener model. The Landau-Zener model describes a single two-level sys-

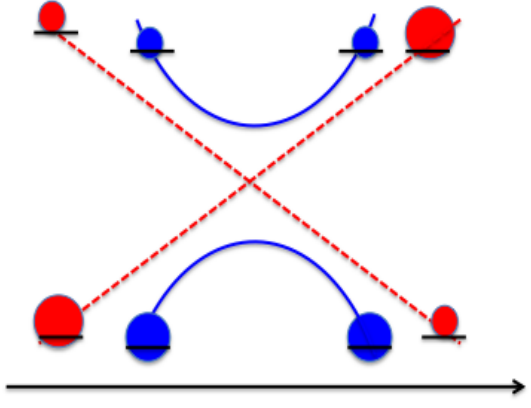


Figure 10. (Color online) We display the population inversion in the case of level crossing by red dotted lines. The populations remain in their energy levels in the avoided crossing regime displayed by blue solid lines.

tem. It is described by the Hamiltonian,

$$H_{LZ} = -\frac{\omega_0}{2} \sigma_z + g \sigma_x, \quad (A1)$$

where σ_x and σ_z are Pauli spin matrices. The gap is given by the parameter g and the transition frequency is ω_0 . For the $g = 0$ case, a spin-1/2 model is retrieved.

The ground state energy is $E_0 = -\frac{1}{2}\sqrt{4g^2 + \omega_0^2}$ and the excited state is given by $E_1 = \frac{1}{2}\sqrt{4g^2 + \omega_0^2}$. The energy spectrum of Eq. (A1) displays two different behaviours, depending on the value of the coupling g : (1) For $g = 0$, it exhibits a level crossing of energy levels at the critical value $\omega_0 = 0$, and (2) for $g \neq 0$, it shows an avoided crossing at the critical value $\omega_0 = 0$. The level crossing gives rise to a first-order quantum phase transition (QPT), while the avoided crossing leads to a second-order QPT [38]. A schematic of these two behaviours of the Landau-Zener model at the critical point is given in Fig. 10.

Next, we show that it is possible to probe QPTs of the Landau-Zener model for both avoided crossing and level crossing via the work output of quantum heat engine cycles. The heat engine operates using a quantum Otto cycle, consisting of quantum adiabatic and quantum isochoric stages, as depicted in Fig. 11. The control parameter in the cycle is the transition frequency ω_0 , which takes values between the hot isochore frequency ω_1 and the cold isochore frequency ω_2 . In the cycle for the spin-1/2 engine, negative temperatures are used to implement population inversion. Consideration of negative temperatures in the context of heat engines and refrigerators to examine the foundations and extent of thermodynamical laws is an old problem [39], which recently has received much attention due to the recognition of the advantages of negative temperatures in quantum thermodynamics [40–44]. The system goes through the following stages for the spin-1/2 engine with $g = 0$ and the Landau-Zener

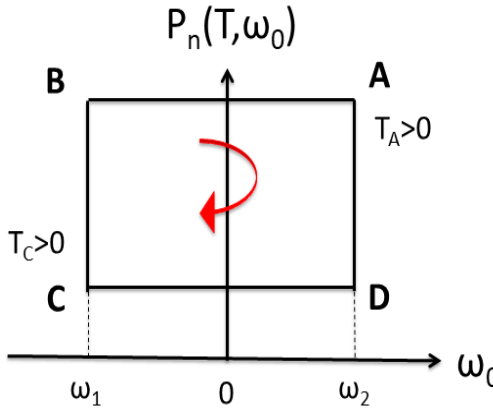


Figure 11. (Color online) Quantum Otto engine scheme (occupation probability-transition frequency, e.g. $P_n(T, \omega) - \omega_0$) for both the spin-1/2 system and the Landau-Zener model with $g \neq 0$ (cycle direction is the same for both cases and is given by the red arrow). The system is in contact with a cold bath at point A and a hot bath at point C. The cold and hot temperatures are $T_A = 0.5$ and $T_C = 2$, respectively. The hot and cold isochore parameter is kept constant at $\omega_0 = \omega_1$ and $\omega_0 = \omega_2$, respectively.

engine with $g = 0.1$ (the cycle direction is the same for the both engines and is given by the red arrow in Fig. 11).

- Stage 1 (A to D): The system is attached to a cold bath with positive temperature at point A, and starts at a thermal state with $\omega_2 > 0$, $T_A > 0$. The system is detached from the cold bath and isochoric heat transfer takes place at fixed $\omega_2 > 0$. The heat Q_α^{in} is injected to the system:

$$Q_\alpha^{\text{in}} = \sum_n E_n(\omega_2) [P_n(T_D, \omega_2) - P_n(T_A, \omega_2)]. \quad (\text{A2})$$

Here, α labels either the spin-1/2 system with 1/2 or the Landau-Zener system with LZ. The spin-1/2 system (Landau-Zener system) attains negative (positive) temperature $T_D < 0$ ($T_D > 0$) at point D.

- Stage 2 (D to C): The system is quantum adiabatically transformed to a thermal state at point C, where it is attached to a hot bath at temperature $T_C > 0$. The system passes through a level crossing (an avoided crossing) point at $\omega_0 = 0$ for the spin-1/2 system (for the Landau-Zener system), as the transition frequency is changed. There is no heat transfer but work is done on the system. A population inversion occurs in the spin-1/2 system as the temperature changes from $T_D < 0$ to $T_C > 0$.
- Stage 3 (C to B): The system is separated from the hot bath. An isochoric heat transfer takes place at fixed $\omega_1 < 0$. The temperature at point B is $T_B < 0$ ($T_B > 0$) for spin-1/2 system (for the Landau-Zener

system). No work is done but heat Q_α^{out} is ejected by the system:

$$Q_\alpha^{\text{out}} = \sum_n E_n(\omega_1) [P_n(T_B, \omega_1) - P_n(T_C, \omega_1)]. \quad (\text{A3})$$

- Stage 4 (B to A): The system is quantum adiabatically transformed to another state at point A passing through the critical point at $\omega_0 = 0$ as the transition frequency is changed from ω_1 to ω_2 . There is no heat transfer but work is done. A population inversion occurs for the spin-1/2 system, as $T_B < 0$ at point B and $T_A > 0$ at point A. For the Landau-Zener system, $T_B > 0$, and the populations remain in their energy levels.

In Eq. (A3) and Eq. (A2),

$$P_n(T_i, \omega_0) = \frac{e^{-\beta_i E_n(\omega_0)}}{Z(T_i, \omega_0)}$$

are the occupation probabilities corresponding to energy $E_n(\omega_0)$ with $n = 1, 2$. i labels the cycle points with $i = A, B, C, D$. $Z(T_i, \omega_0) = \sum_n e^{-\beta_i E_n(\omega_0)}$ is the partition function. $\beta_i = 1/(k_B T_i)$, where $k_B = 1$ is the Boltzmann constant.

Fig. 12a displays the incoming heat $Q_{1/2}^{\text{in}}$, outgoing heat $Q_{1/2}^{\text{out}}$ and work output $W_{1/2}$ of the spin-1/2 quantum heat engine working between a cold bath at temperature $T_A = 0.5$ and a hot bath at temperature $T_C = 2$. The system is prepared at point A with $\omega_0 = \omega_2 = 2$. Fig. 12b displays the incoming heat $Q_{\text{LZ}}^{\text{in}}$, outgoing heat $Q_{\text{LZ}}^{\text{out}}$ and work output W_{LZ} of the Landau-Zener quantum heat engine in its avoided crossing regime.

In Fig 13, we show the boundary and bulk contributions in the Kitaev heat engine, which uses an ideal Otto cycle. We consider a Kitaev chain of length $n = 225$ with a superconducting pairing parameter $\Delta = 0.25$ as in the rest of the paper with the same cold and hot bath temperatures, $T_A = 0.05$ and $T_C = 0.08$, respectively. The chemical potential is fixed at $\mu = 0.5$, and the hopping parameter t is used as the control parameter for which a topological phase transition (TPT) takes place at $t = 0.25$. For such an ideal Otto cycle, the first isochore parameter t_1 is changed, while the parameter of the second isochore t_2 is held fixed at 0.3. The cycle direction is the same as in Fig. 1. We specifically choose the control parameter for the topological engine as the hopping parameter t because its function in the finite-length Kitaev chain Hamiltonian, Eq. 12 is comparable with the function of the transition probability parameter ω_0 in the Landau-Zener Hamiltonian given in Eq. A1.

The behavior for the case of the spin-1/2 model depicted in Fig. 12a is qualitatively the same as the one found in Fig. 13a for the boundary contribution in the topological Kitaev chain engine. The spin-1/2 model captures the first-order quantum phase transition nature of the topological phase transition at the boundary. There,

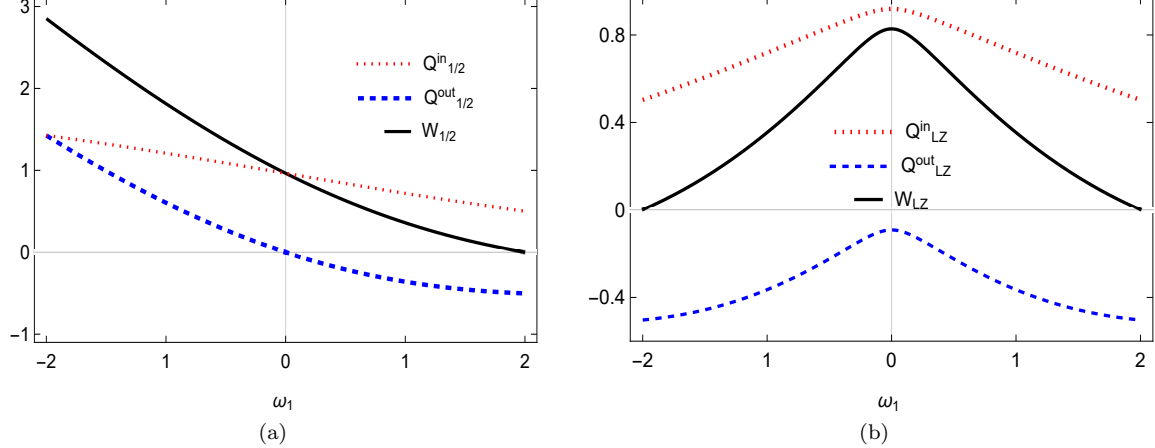


Figure 12. (Color online) (a) Incoming heat $Q_{1/2}^{\text{in}}$ (red dotted), outgoing heat $Q_{1/2}^{\text{out}}$ (blue dashed) and work output $W_{1/2}$ (black solid) for a spin-1/2 system, and (b) incoming heat $Q_{\text{LZ}}^{\text{in}}$ (red dotted), outgoing heat $Q_{\text{LZ}}^{\text{out}}$ (blue dashed) and work output W_{LZ} (black solid) for the Landau-Zener model with $g = 0.1$, are given as a function of ω_1 of the hot isochore. The initial transition frequency $\omega_0 = \omega_2 = 2$ is held fixed and ω_1 is changed in the figure.

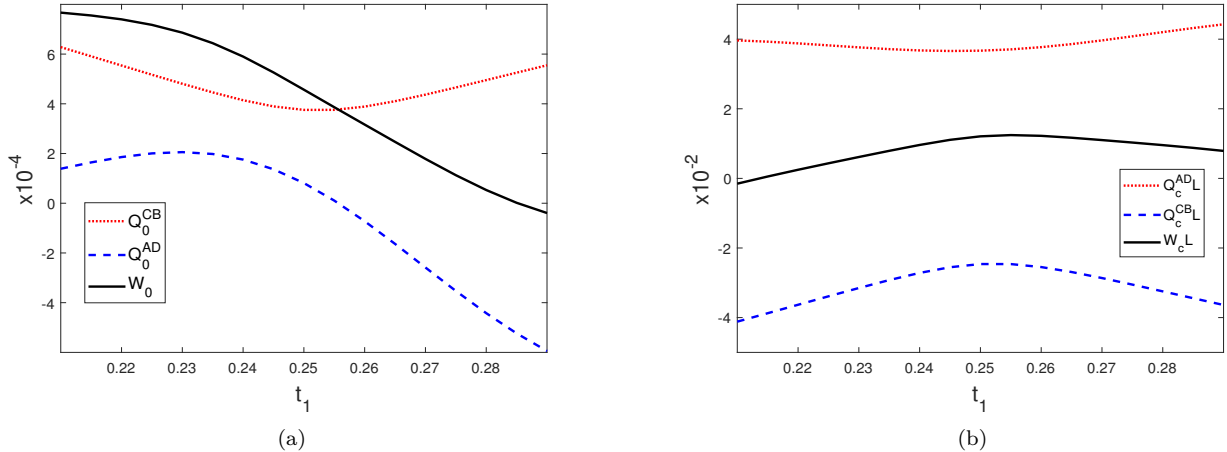


Figure 13. (Color Online) (a) The boundary and (b) the bulk contributions to the injected Q_0^{in} , Q_c^{in} (blue dashed) and ejected heat, Q_0^{out} , Q_c^{out} (red dotted), and to the work output W_0 , W_c (black solid), respectively, as a function of the hopping parameter t_1 of the first isochore of a finite-length Kitaev chain in an Otto cycle, operating between a cold bath at temperature $T_A = 0.05$ and a hot bath at temperature $T_C = 0.08$. The control parameter of the engine is t_1 , which changes from 0.2 to 0.3.

the emergence of unpaired Majorana fermions can be considered as two uncoupled spins for an intuitive description of the heat and work behavior in Fig. 13a.

The intersection of $Q_{1/2}^{\text{in}}$ and $W_{1/2}$ in Fig. 12a is also a common feature in the heat and the work behaviour of spin-1/2 and the boundary of Kitaev chain systems, which occurs due to the fact that $Q_{1/2}^{\text{out}} = 0$. No heat transfer is required to equilibrate the system with the bath at T_C , as both levels are degenerate at the transition point ($\omega_0 = 0$ in Fig. 12a and $t_1 = 0.25$ in Fig. 13a). Another common feature is that the thermal cycle characteristics before and after the phase transition are different both in Fig. 12a and in Fig. 13a: Before their respective transition points, their

thermal cycles cannot be identified with a heat engine or a heat pump, but after the phase transition point, they both operate as heat engines producing positive work.

The Landau-Zener engine also operates according to the scheme given in Fig. 11. We note that the temperatures at T_B and T_D are positive for such an engine, since the system is taken through an avoided crossing point at $\omega_0 = 0$. The assignment of negative temperatures is used only when there is a population inversion in the system.

The behavior of Fig. 13b, which is the bulk contribution to the topological Kitaev heat engine, is captured by Landau-Zener quantum engine results depicted in Fig. 12b. Both results are consistent with the second-order nature of the phase transitions. The work output is maximized at

the critical point, at $\omega_1 = 0$ for the Landau Zener quantum heat engine and at $t_1 = 0.25$ for the bulk contribution of the topological finite Kitaev heat engine. Before and after their respective critical points, the thermal cycles can be properly identified as heat engines.

Thus, we report that thermal cycles display universal features in their heat exchange and work output behaviours according to the order of phase transition taking place.

[1] Terrell L. Hill, *Thermodynamics of Small Systems* (Courier Corporation, 1964).

[2] Terrell L. Hill, “Thermodynamics of small systems, part i,” *Isr. J. Chem.* **3**, 39–39 (1965).

[3] R. V. Chamberlin, “The big world of nanothermodynamics,” *Entropy* **17**, 52–73 (2015).

[4] Terrell L. Hill, “Perspective : Nanothermodynamics,” *Nano Lett.* **1**, 111–112 (2001).

[5] Terrell L. Hill, “A different approach to nanothermodynamics,” *Nano Lett.* **1**, 273–275 (2001).

[6] A. Quelle, E. Cobanera, and C. Morais Smith, “Thermodynamic signatures of edge states in topological insulators,” *Phys. Rev. B* **94**, 075133 (2016).

[7] S. N. Kempkes, A. Quelle, and C. Morais Smith, “Universality of thermodynamic signatures in topological phases,” *Sci. Rep.* **6**, 38530 (2016).

[8] O. Viyuela, A. Rivas, and M. A. Martin-Delgado, “Two-dimensional density-matrix topological fermionic phases: Topological Uhlmann numbers,” *Phys. Rev. Lett.* **113**, 076408 (2014).

[9] O. Viyuela, A. Rivas, and M. A. Martin-Delgado, “Uhlmann phase as a topological measure for one-dimensional fermion systems,” *Phys. Rev. Lett.* **112**, 130401 (2014).

[10] M. Rivás and M. A. Martin-Delgado, “Topological heat transport and symmetry-protected boson currents,” *Sci. Rep.* **7**, 6350 (2017).

[11] J. J. van den Broeke, S. N. Kempkes, A. Quelle, X. F. Wang, J. Paglione, and C. Morais Smith, “Thermodynamic study of topological Kondo insulators,” [arXiv:1803.03553](https://arxiv.org/abs/1803.03553) (2018).

[12] M. Fadaie, E. Yunt, and Ö. E. Müstecaplıoğlu, “Topological phase transition in quantum-heat-engine cycles,” *Phys. Rev. E* **98**, 052124 (2018).

[13] A. Y. Kitaev, “Unpaired Majorana fermions in quantum wires,” *Physics-Uspekhi* **44**, 131–136 (2001).

[14] A. Y. Kitaev, “Fault-tolerant quantum computation by anyons,” *Ann. Phys.* **303**, 2 – 30 (2003).

[15] J. Alicea, “New directions in the pursuit of Majorana fermions in solid state systems,” *Rep. Prog. Phys.* **75**, 076501 (2012).

[16] P. Molignini, E. van Nieuwenburg, and R. Chitra, “Sensing Floquet-Majorana fermions via heat transfer,” *Phys. Rev. B* **96**, 125144 (2017).

[17] E. W. Elcock and P. T. Landsberg, “Temperature dependent energy levels in statistical mechanics,” *Proc. Phys. Soc., B* **70**, 161–168 (1957).

[18] G. S. Rushbrooke, “On the statistical mechanics of assemblies whose energy-levels depend on the temperature,” *Trans. Faraday Soc.* **36**, 1055–1062 (1940).

[19] R. de Miguel and J. M. Rubí, “Finite systems in a heat bath: Spectrum perturbations and thermodynamics,” *J. Phys. Chem. B* **120**, 9180–9186 (2016).

[20] R. de Miguel and J. M. Rubí, “Thermodynamics far from the thermodynamic limit,” *J. Phys. Chem. B* **121**, 10429–10434 (2017).

[21] R. de Miguel, “Temperature-dependent energy levels and size-independent thermodynamics,” *Phys. Chem. Chem. Phys.* **17**, 15691–15693 (2015).

[22] T. Yamano, “Efficiencies of thermodynamics when temperature-dependent energy levels exist,” *Phys. Chem. Chem. Phys.* **18**, 7011–7014 (2016).

[23] T. Yamano, “Effect of temperature-dependent energy levels on exergy,” *J. Phys. Commun.* **1**, 055007 (2017).

[24] O. Shental and I. Kanter, “Shannon meets Carnot: Generalized second thermodynamic law,” *EPL (Europhysics Letters)* **85**, 10006 (2009).

[25] Ronnie Kosloff and Tova Feldmann, “Discrete four-stroke quantum heat engine exploring the origin of friction,” *Phys. Rev. E* **65**, 055102 (2002).

[26] J. L. Lebowitz and J. K. Percus, “Thermodynamic Properties of Small Systems,” *Phys. Rev.* **124**, 1673–1681 (1961).

[27] A. Aydin and A. Sisman, “Quantum shape effects and novel thermodynamic behaviors at nanoscale,” *Phys. Lett. A* **383**, 655 – 665 (2019).

[28] D. Bedeaux and S. Kjelstrup, “Hill’s nanothermodynamics is equivalent with Gibbs’ thermodynamics for surfaces of constant curvatures,” *Chem. Phys. Lett.* **707**, 40–43 (2018).

[29] Y.P. Varshni, “Temperature dependence of the energy gap in semiconductors,” *Physica* **34**, 149 – 154 (1967).

[30] D. Emin, “Effect of temperature-dependent energy-level shifts on a semiconductor’s Peltier heat,” *Phys. Rev. B* **30**, 5766–5770 (1984).

[31] P. B. Allen and V. Heine, “Theory of the temperature dependence of electronic band structures,” *J. Phys. C: Solid State Phys.* **9**, 2305–2312 (1976).

[32] C. E. Patrick and F. Giustino, “Unified theory of electron–phonon renormalization and phonon-assisted optical absorption,” *J. Phys.: Condens. Matter* **26**, 365503 (2014).

[33] M. I. Dykman, K. Kono, D. Konstantinov, and M. J. Lea, “Ripplonic Lamb shift for electrons on liquid helium,” *Phys. Rev. Lett.* **119**, 256802 (2017).

[34] M. Kolář, A. Ryabov, and R. Filip, “Optomechanical oscillator controlled by variation in its heat bath temperature,” *Phys. Rev. A* **95**, 042105 (2017).

[35] M. Kolář, A. Ryabov, and R. Filip, “Heat capacities of thermally manipulated mechanical oscillator at strong coupling,” *Sci. Rep.* **9**, 10885 (2019).

[36] U. Seifert, “First and Second Law of Thermodynamics at Strong Coupling,” *Phys. Rev. Lett.* **116**, 020601 (2016).

[37] P. Talkner and P. Hänggi, “Open system trajectories specify fluctuating work but not heat,” *Phys. Rev. E* **94**, 022143 (2016).

[38] E. Mascarenhas, H. Bragança, R. Dorner, M. França Santos, V. Vedral, K. Modi, and J. Goold, “Work and quantum phase transitions: Quantum latency,” *Phys. Rev.*

E **89**, 062103 (2014).

[39] P. T. Landsberg, “Heat engines and heat pumps at positive and negative absolute temperatures,” *J. Phys. A: Math. Gen* **10**, 1773–1770 (1977).

[40] F. Tacchino, A. Auffèves, M. F. Santos, and D. Gerace, “Steady state entanglement beyond thermal limits,” *Phys. Rev. Lett.* **120**, 063604 (2018).

[41] H. Struchtrup, “Work storage in states of apparent negative thermodynamic temperature,” *Phys. Rev. Lett.* **120**, 250602 (2018).

[42] R. J. de Assis, T. M. de Mendonça, C. J. Villas-Boas, A. M. de Souza, R.S. Sarthour, I. S. Oliveira, and N. G. de Almeida, “Efficiency of a quantum Otto heat engine operating under a reservoir at effective negative temperatures,” *Phys. Rev. Lett.* **122**, 240602 (2019).

[43] J-Y. Xi and H-T. Quan, “Quantum heat engine and negative Boltzmann temperature,” *Commun. Theor. Phys.* **68**, 347 (2017).

[44] M. Campisi, “Notes on heat engines and negative temperatures,” [arXiv:1606.05244](https://arxiv.org/abs/1606.05244).